Identifying the Mechanism of Biosensing with Carbon Nanotube Transistors

ARTICLE *in* NANO LETTERS · MARCH 2008

Impact Factor: 13.59 · DOI: 10.1021/nl072996i · Source: PubMed

6 AUTHORS, INCLUDING:

Iddo Heller
VU University Amsterdam
35 PUBLICATIONS **1,056** CITATIONS

SEE PROFILE

NANO LETTERS

2008
Vol. 8, No. 2
591−595

Identifying the Mechanism of Biosensing with Carbon Nanotube Transistors

Iddo Heller, Anne M. Janssens, Jaan Männik, Ethan D. Minot,† Serge G. Lemay, and Cees Dekker*

Kavli Institute of Nanoscience, Delft University of Technology, Lorentzweg 1, 2628 CJ Delft, The Netherlands

Received November 16, 2007; Revised Manuscript Received December 1, 2007

ABSTRACT

Carbon nanotube transistors have outstanding potential for electronic detection of biomolecules in solution. The physical mechanism underlying sensing however remains controversial, which hampers full exploitation of these promising nanosensors. Previously suggested mechanisms are electrostatic gating, changes in gate coupling, carrier mobility changes, and Schottky barrier effects. We argue that each mechanism has its characteristic effect on the liquid gate potential dependence of the device conductance. By studying both the electron and hole conduction, the sensing mechanisms can be unambiguously identified. From extensive protein-adsorption experiments on such devices, we find that electrostatic gating and Schottky barrier effects are the two relevant mechanisms, with electrostatic gating being most reproducible. If the contact region is passivated, sensing is shown to be dominated by electrostatic gating, which demonstrates that the sensitive part of a nanotube transistor is not limited to the contact region, as previously suggested. Such a layout provides a reliable platform for biosensing with nanotubes.

Nanoscale semiconducting materials such as carbon nanotubes[1−21] or nanowires[22−24] show great potential for use as highly sensitive electronic biosensors. Single-walled carbon nanotubes (SWNTs) arguably are the ultimate biosensor in this class for a number of reasons: SWNTs have the smallest diameter (∼1 nm), directly comparable to the size of single biomolecules and to the electrostatic screening length in physiological solutions.[6,25] Furthermore, the low charge-carrier density of SWNTs[26] is directly comparable to the surface charge density of proteins,[27] which intuitively makes SWNTs well suited for electronic detection that relies on electrostatic interactions with analyte biomolecules. Finally, the SWNT consists solely of surface such that every single carbon atom is in direct contact with the environment, allowing optimal interaction with nearby biomolecules. Although an appreciable amount of biosensing studies has been conducted using carbon nanotube transistors, the physical mechanism that underlies sensing is still under debate.[21] Previously suggested mechanisms are electrostatic gating,[1−3] changes in gate coupling,[4] carrier mobility changes,[5,6] and Schottky barrier effects.[3,7−9] The lack of a good understanding of the sensing mechanism hampers the further exploitation of these promising nanosensors.

In this report, we resolve the issue of the sensing mechanism through both extensive protein-adsorption experiments and modeling. We show that studying the effect of protein adsorption on the liquid gate potential dependence of device conductance can yield unambiguous information on the sensing mechanism, particularly in cases where devices reveal ambipolar conduction. From extensive protein adsorption experiments, we find that sensing is dominated by a combination of electrostatic gating and Schottky barrier effects, where the electrostatic gating effect is most reproducible. Finally, we show that by passivating the SWNT−metal contacts, the unreliable Schottky barrier effect can be suppressed, predominantly leaving the electrostatic gating effect caused by the charge of nearby biomolecules.

SWNTs were grown on thermally oxidized silicon wafers by chemical vapor deposition from patterned alumina-supported iron catalyst, followed by deposition of lithographically defined Ti or Cr/Au electrodes. Figure 1a shows a semiconducting SWNT employed in a field-effect transistor layout.[28] A home-built flow-cell is placed over the SWNT device to control the liquid environment that consists of various solutions buffered by 10 mM phosphate buffer (PB) at pH 7.2. The conductance of a SWNT transistor submerged in an electrolyte can be tuned using the electrolyte as a highly effective gate as schematically depicted in Figure 1b.[29] A liquid gate potential is applied to a reference electrode with

* Corresponding author. E-mail: c.dekker@tudelft.nl.
† Present address: Department of Physics, Oregon State University, 301 Weniger Hall, Corvallis, Oregon 97331-6507.

10.1021/nl072996i CCC: $40.75
Published on Web 12/28/2007

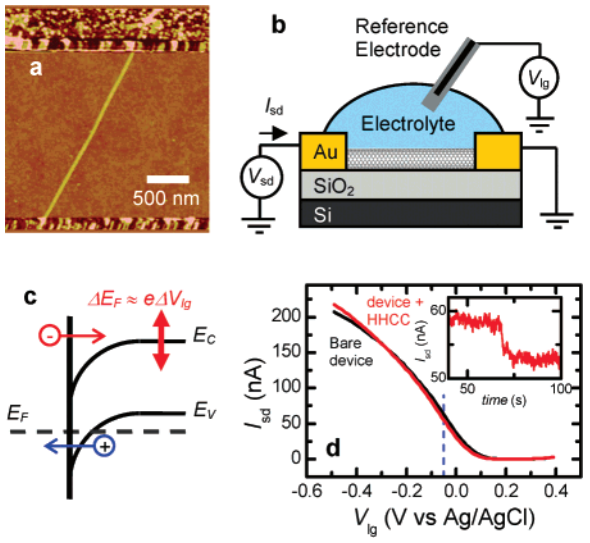

Figure 1. Experimental layout and results of a typical biosensing experiment. (a) Atomic force microscopy topology image of a SWNT between Cr/Au contacts on an insulating SiO_2 substrate. (b) Measurement setup, where a source-drain bias potential is applied and the device is gated through an Ag/AgCl reference electrode inserted in the electrolyte. The electrolyte is contained in a home-built flow cell (not depicted). (c) Band diagram for a hole-doped SWNT showing electron conduction through thermally activated carriers into conductance band and hole conduction through tunneling through the Schottky barrier. E_F is the Fermi-energy. E_C and E_V are the energies of SWNT conductance and valence band edges respectively. The liquid gate potential changes the doping level in the bulk of the SWNT as indicated by the red arrows. (d) Results of a typical biosensing experiment. Current versus liquid gate potential curves acquired before (black line) and after (red line) adsorption of 1 μM HHCC in PB buffer ($V_{sd} = 10$ mV). The inset shows the real-time drop in conductance when HHCC is flushed over the device, while the gate potential is held constant at −50 mV vs Ag/AgCl, (as indicated by the blue dashed line).

respect to the grounded drain electrode, while a small (10 mV) bias voltage is applied over source and drain electrodes to monitor device conductance. To create a well-defined, stable gate potential[10] and avoid sensing artifacts as pointed out by Minot et al.,[16] we use an Ag/AgCl (3M NaCl) reference electrode (BioAnalytical Systems).

The black solid line in Figure 1d shows a typical source-drain current (I) versus liquid gate potential (V_{lg}) curve recorded in a buffer solution. Because of the high mobility of charge carriers in SWNTs,[30] the device conductance is limited by the Schottky barriers that form at the metal−nanotube contacts (cf. Figure 1c).[31,32] We can thus approximate the device conductance using a model for the shape of the Schottky barrier, taken as the electrostatic potential profile in the electrical double-layer, as a function of V_{lg} (Supporting Information).[26,31]

A typical biosensing experiment is shown in the inset of Figure 1d. Because of the high sensitivity of the SWNT to the liquid gate potential, that is, to its electrostatic environment, a small electrostatic disturbance caused by nearby biomolecules can lead to a significant change in device conductance. The inset in Figure 1d shows the real-time drop in device conductance measured at constant $V_{lg} = -50$ mV when a buffered solution of 1 μM horse heart cytochrome-c (HHCC, positive charge at pH 7.2) is flushed over the device, allowing proteins to adsorb on SWNT device and the SiO_2 substrate (see Supporting Information, Figure S1). This drop in conductance directly corresponds to the change of the $I-V_{lg}$ characteristics from the black to the red curve in Figure 1d, acquired respectively before and after the addition of HHCC.

Figure 1d strikingly demonstrates the importance of V_{lg}: the $I-V_{lg}$ curves acquired before and after protein adsorption cross at $V_{lg} = -300$ mV. This implies that depending on the potential at which V_{lg} is fixed during a real-time protein adsorption experiment, the magnitude and even sign of the conductance change may vary. This necessitates reliable and judicious control of liquid gate potential,[16] and complicates direct quantitative and qualitative interpretation of SWNT sensor experiments. We will show that a better understanding of the effect of protein adsorption on $I-V_{lg}$ characteristics allows us to interpret the changes in Figure 1d as a combination of electrostatic gating and Schottky barrier effects.

We can use the $I-V_{lg}$ curves as a tool to identify the sensing mechanism: Figure 2 illustrates the characteristic qualitative effect of protein adsorption on $I-V_{lg}$ curve for each previously mentioned sensing mechanism. (The curves are calculated using the model described in the Supporting Information.) In Figure 2a, we show the change in the $I-V_{lg}$ curve in the case of electrostatic gating by adsorbed charged species that induce a screening charge (doping) in the SWNT thus shifting the $I-V_{lg}$ curve along the voltage axis.[1,2] This situation also describes the effect of partial charge transfer.[11] Note that adsorption of a positively charged species induces additional negative charge in the SWNT, thus n-doping the SWNT and shifting the $I-V_{lg}$ curve toward more negative gate voltages. (The opposite holds for negatively charged adsorbents.) To illustrate the charge sensitivity, we estimate that a change in charge of merely 0.003 e per nanometer length of SWNT induces about 1 mV shift in V_{lg}, assuming an interfacial capacitance of ∼0.4 nF per unit length of nanotube in the on-state.[26,29]

Figure 2b shows the Schottky barrier mechanism as suggested Chen et al.[7] where adsorbed biomolecules at the metal contact modulate the local workfunction and thus the band alignment. Because the Schottky barrier height changes in opposite directions for hole (p) and electron (n) transport (see insets), a characteristic asymmetric conductance change for p- and n-branches of $I-V_{lg}$ curves is obtained.

Figure 2c shows the effect of a reduced gate efficiency, which may occur when the gate capacitance is reduced due to low permittivity ϵ of adsorbed biomolecules relative to the electrolyte.[4,18] Because the SWNT electrolyte interfacial capacitance is normally dominated by the SWNT quantum capacitance,[29] the electrostatic capacitance reduction due to adsorbed biomolecules can only become apparent in case of near-full coverage under the disputable assumption that ions cannot permeate through this protein layer.[26]

Finally, Figure 2d shows the effect of reduced carrier mobility,[6] suppressing the conductance in both p- and

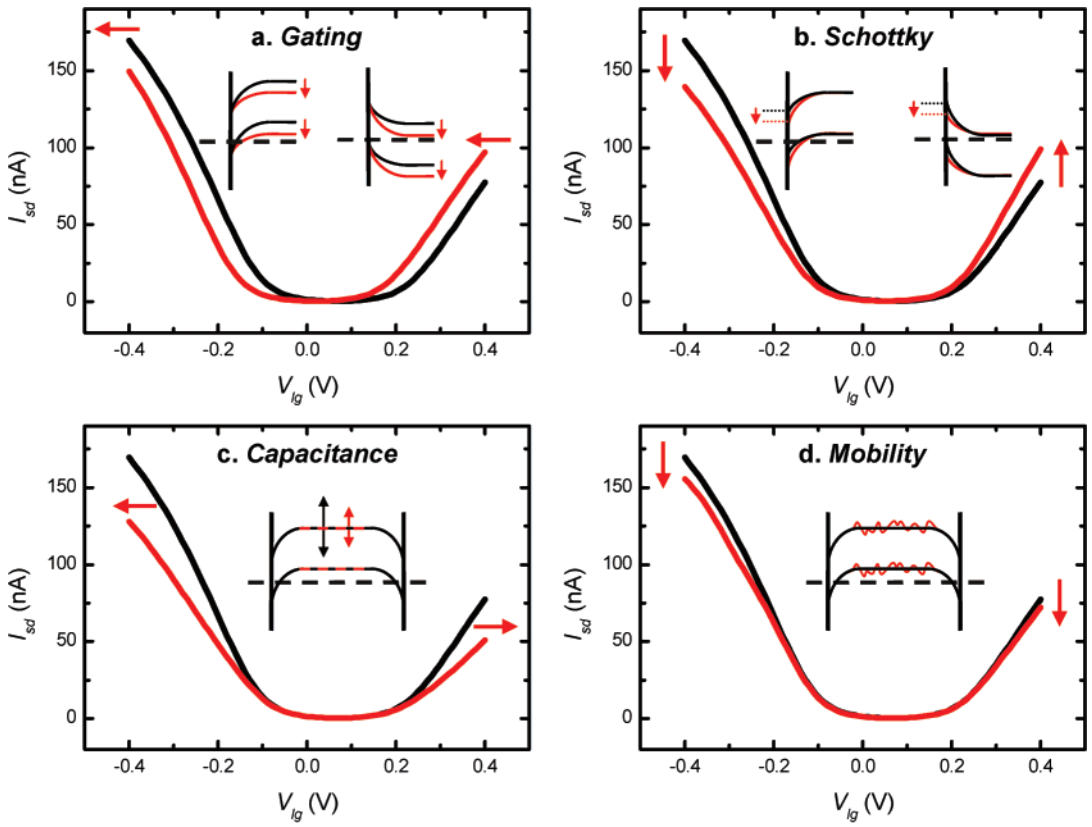

Figure 2. Calculated $I-V_{lg}$-curves before (black) and after (red) protein adsorption for four different sensing mechanisms. The bias voltage is 10 mV. (a) Electrostatic gating effect corresponding to a 50 meV shift of the semiconducting bands downward. (b) Schottky barrier effect that corresponds to a change of the difference between metal and SWNT workfunctions of 30 meV. In panels a and b, left and right insets illustrate the corresponding changes in the band diagrams for hole and electron doping respectively. (c) Capacitance mechanism for a 90% coverage of SWNT with protein ($\epsilon = 10$, diameter = 6 nm). In panels c and d, the insets illustrate the corresponding changes in the band diagrams. (d) Mobility mechanism that corresponds to a mobility reduction to a mere 2% of the initial value.

n-branches. Because transport in Schottky barrier SWNT transistors is in general not limited by diffusive transport due to their extremely high carrier mobility,[30] this mechanism is unlikely to dominate sensing. Supporting Information shows that a significant change of $I-V_{lg}$ curves is only obtained in the case of dramatically reduced carrier mobility (e.g., by 98% for curves in Figure 2d).

To identify the sensing mechanism experimentally, we extensively studied changes in $I-V_{lg}$ curves for a large number of devices. We observed a range of characteristic $I-V_{lg}$ changes. For illustration, Figure 3a,b shows two extreme cases of observed behavior that we can directly identify as electrostatic gating and Schottky barrier modulation, respectively. Figure 3a shows that after flushing a 185 nM poly-L-lysine (PLL) solution, the entire $I-V_{lg}$ curve shifts 100 mV toward negative gate potential. This shift is induced by the high positive charge of PLL (at pH 7.2) that causes n-doping in the SWNT. Because both p- and n-branches are shifted, the dominant mechanism is unambiguously electrostatic gating. Figure 3b shows the other extreme of observed $I-V_{lg}$ changes. After flushing a 1 μM HHCC solution, a clear drop in hole conduction (ΔG_P) and concomitant increase in electron conduction (ΔG_N) is observed, corresponding to an increase in metal work function.[7,8] To our knowledge, this represents the most direct observation of the workfunction modulation mechanism in SWNTs to date. Figure S3 in Supporting Information shows a similarly large workfunction change obtained with another biomolecule. All devices showed the gating and/or Schottky effects; we did not systematically observe the capacitance or mobility mechanisms. This conclusion is consistent with a recent report of DNA immobilization on back-gated SWNT networks.[3]

To gain insight in the device-to-device variability of the sensing mechanism, Figure 3c shows a histogram of the shift of the $I-V_{lg}$ curve, V_{shift} after adsorption of 1 μM HHCC (see Supporting Information for method of analyzing V_{shift}) yielding a consistently negative doping $V_{shift} = -25$ mV $\pm$ 18 mV (20 devices). After correcting for V_{shift}, we compare ΔG_P and ΔG_N at the opposite extreme endpoints of the measured V_{lg} range as plotted in Figure 3d. (In Figure S4 in Supporting Information, we show ΔG_P versus ΔG_N averaged over the entire V_{lg} range, yielding essentially the same results.) Although 2 out of 15 ambipolar devices are positioned in the hatched ($\Delta G_N < 0$) and ($\Delta G_P < 0$) quadrant, corresponding to mobility and/or capacitance mechanisms, the majority of devices appears consistent with Schottky barrier modulation as roughly indicated by the line $\Delta G_N = -\Delta G_P$. Contrary to the more reliable electrostatic gating shift, the apparent workfunction−modulation strongly varies from device to device over a range of both positive and negative values. We speculate that this is related to the nanometer scale of the metal−SWNT contact, which can be

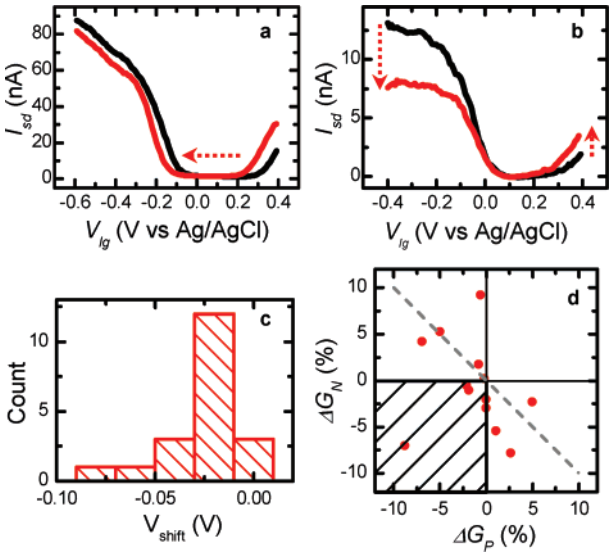

Figure 3. Changes in liquid gate sweeps of ambipolar devices measured during protein adsorption experiments. (a) Example of strong electrostatic gating (adsorption of 185 nM poly-L-lysine on an ambipolar SWNT device). (b) Example of a strong Schottky barrier effect in the case of adsorption of 1 μM HHCC on a short (40 nm) SWNT device. (c) Histogram of V_{shift} for 20 HHCC adsorption experiments yielding $V_{shift} = -25 \pm 18$ mV. (d) Scatterplot of the changes in p- and n-conductance (ΔG_N and ΔG_P, respectively) after HHCC adsorption on ambipolar devices, taken at the opposite extreme points of the V_{lg} range, after the data has been corrected for the electrostatic gating shift. The hatched ($\Delta G_N < 0$) and ($\Delta G_P < 0$) quadrant represents mobility and capacitance mechanisms, while the dashed line $\Delta G_N = -\Delta G_P$ roughly indicates the Schottky barrier mechanism. Figure S2 of Supporting Information shows the dataset on a larger scale with two more datapoints.

affected either way by positively or negatively charged regions of HHCC, depending on protein orientation. Furthermore, the contact region is prone to subtle variations in device fabrication such as level of oxidation of adhesion layers and pile-up of wet-processing residues.

From the experiments in Figure 3, we conclude that both electrostatic gating and Schottky barrier modulation are responsible for changes in $I-V_{lg}$ curves. We can go further and use the previously mentioned model to extract quantitative information. For example, by modeling the $I-V_{lg}$ curves of Figure 1d (see Supporting Information, Figure S5), we find that HHCC adsorption in this experiment can be well described by the combination of an electrostatic gating effect of -33 mV and a metal work function change of 16 meV.

A crucial issue for design and applications of SWNT sensors concerns the region of the device where protein adsorption causes significant conductance changes. Although earlier reports, which suggest workfunction modulation to be the dominant sensing mechanism,[7,8] imply that the sensitive region is limited to the nanoscale contact regions, our results clearly indicate that in addition, strong electrostatic gating reliably occurs along the bulk of the SWNT channel. To explicitly confirm this important result, we fabricated poly(methyl-metacrylate) (PMMA) contact-passivated devices, where solution-access is restricted to an exposed region along the bulk of the SWNT[19] (see upper inset Figure 4a). Because addition of PLL (red curve) to the contact-passivated

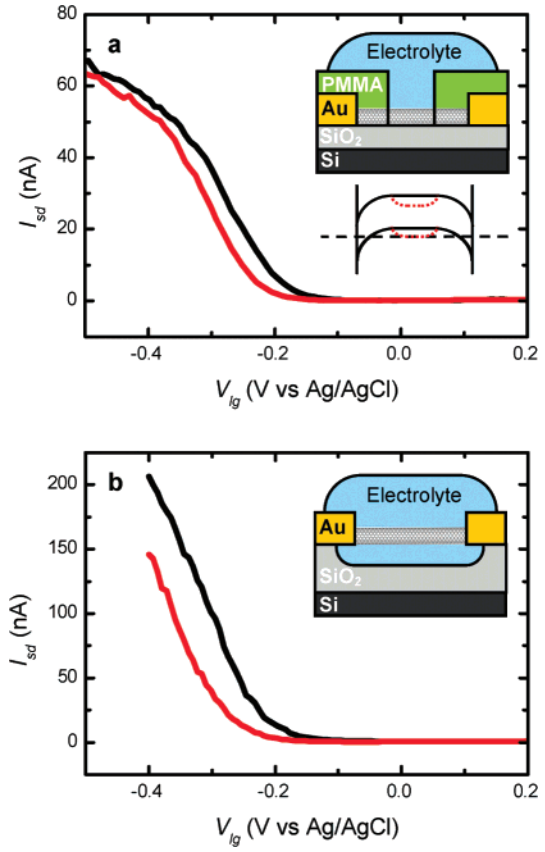

Figure 4. $I-V_{lg}$ curves before (black) and after (red) PLL adsorption on modified SWNT devices. (a) 200 nM PLL adsorption on a SWNT device where the electrodes and contact area are passivated by PMMA. Top and bottom insets illustrate device architecture and band-diagram changes upon protein adsorption, respectively. (b) 185 nM PLL adsorption on a suspended SWNT device. The inset illustrates the device geometry.

device yields a clear 70 mV shift in $I-V_{lg}$ curve, we can unambiguously conclude that work function modulation at the metal−SWNT contact cannot be responsible for this change in $I-V_{lg}$ curve.[7,8] This directly implies that sensing is not limited to the contacts, but extends to the bulk channel section of the SWNT.

A second important issue for protein sensing is whether this shift can be directly related to the charge of the biomolecules. Alternatively, an additional shift, unrelated to the protein charge, may occur when the electrolyte surrounding a SWNT is replaced by adsorbed biomolecules that locally change charge screening and the electrostatic coupling between the nearby SiO_2 charge and the SWNT.[2,4] To confirm that a shift indeed originates from the charge of the biomolecules, the experiment was repeated with a suspended SWNT, fabricated by underetching the SiO_2 in buffered HF, where the distance between SWNT channel and substrate is much larger than the Debye screening length in solution. Figure 4b shows an electrostatic gating shift that can now be entirely attributed to PLL adsorbing on the SWNT. In addition, this result indicates that while the substrate may influence biosensing experiments, it is not a necessary element in sensing.

In summary, we have studied the effect of protein adsorption on $I-V_{lg}$ curves. Changes in $I-V_{lg}$ curves can be

used to experimentally identify sensing mechanisms. The identification of mechanisms can be performed unambiguously for the case of SWNT devices that exhibit ambipolar conduction. We find that the majority of our experiments can be explained by a combination of electrostatic gating and Schottky barrier effects. Because these two mechanisms have different gate-potential dependence, the choice of gate potential can strongly affect the outcome of real-time biosensing experiments. Moreover, the Schottky barrier effect at the contact appears less consistent and less reproducible than the electrostatic gating effect along the SWNT bulk. Because passivation of metal−SWNT contacts inhibits signals due to metal work function modulation, predominantly leaving signals from electrostatic gating, contact-passivated devices can provide a reliable platform for biosensors that consist of a single or few SWNT transistors.

Acknowledgment. The authors wish to thank Bernard F. Erlanger for providing the antifullerene antibodies that were used in the Supporting Information. This work was supported by the Stichting voor Fundamenteel Onderzoek der Materie (FOM), the Nederlandse Organisatie voor Wetenschappelijk Onderzoek (NWO), and NanoNed.

Supporting Information Available: Model and parameters used to calculate $I-V_{lg}$ curves, AFM images of cytochrome-*c* adsorption on SWNTs, adsorption experiment with antifullerene antibodies, and additional methods and results of data analysis.

References

(1) Boussaad, S.; Tao, N. J.; Zhang, R.; Hopson, T.; Nagahara, L. A. *Chem. Commun.* **2003**, *13*, 1502−1503.
(2) Artyukhin, A. B.; Stadermann, M.; Friddle, R. W.; Stroeve, P.; Bakajin, O.; Noy, A. *Nano Lett.* **2006**, *6*, 2080−2085.
(3) Gui, E. L.; Li, L. J.; Zhang, K.; Xu, Y.; Dong, X.; Ho, X.; Lee, P. S.; Kasim, J.; Shen, Z. X.; Rogers, J. A.; Mhaisalkar, S. G. *J. Am. Chem. Soc*. **2007**, *129*, 14427−14432.
(4) Besteman, K.; Lee, J. O.; Wiertz, F. G. M.; Heering, H. A.; Dekker, C. *Nano Lett.* **2003**, *3*, 727−730.
(5) Hecht, D. S.; Ramirez, R. J. A.; Briman, M.; Artukovic, E.; Chichak, K. S.; Stoddart, J. F.; Grüner, G. *Nano Lett.* **2006**, *6*, 2031−2036.
(6) Maroto, A.; Balasubramanian, K.; Burghard, M.; Kern, K. *ChemPhysChem*, **2007**, *8*, 220−223.
(7) Chen, R. J.; Choi, H. C.; Bangsaruntip, S.; Yenilmez, E.; Tang, X.; Wang, Q.; Chang, Y. L.; Dai, H. *J. Am. Chem. Soc.* **2004**, *126*, 1563−1568.
(8) Byon, H. R.; Choi, H. C. *J. Am. Chem. Soc.* **2006**, *128*, 2188−2189.
(9) Tang, X.; Bansaruntip, S.; Nakayama, N.; Yenilmez, E.; Chang, Y. L.; Wang, Q. *Nano Lett.* **2006**, *6*, 1632−1636.
(10) Larrimore, L.; Nad, S.; Zhou, X.; Abruña, H.; McEuen, P. L. *Nano Lett.* **2006**, *6*, 1329−1333.
(11) Bradley, K.; Briman, M.; Star, A.; Grüner, G. *Nano Lett.* **2004**, *4*, 253−256.
(12) So, H. M.; Won, K.; Kim, Y. H.; Kim, B. K.; Ryu, B. H.; Na, P. S.; Kim, H.; Lee, J. O. *J. Am. Chem. Soc.* **2005**, *127*, 11906−11907.
(13) Park, D. W.; Kim, Y. H.; Kim, B. S.; So, H. M.; Won, K.; Lee, J. O.; Kong, K. J.; Chang, H. *J. Nanosci. and Nanotechnol.* **2006**, *6*, 3499−3502.
(14) Kojima, A.; Hyon, C. K.; Kamimura, T.; Maeda, M.; Matsumoto, K. *Jpn. J. Appl. Phys.* **2005**, *44*, 1596−1598.
(15) Maehashi, K.; Katsura, T.; Kerman, K.; Takamura, Y.; Matsumoto, K.; Tamiya, E. *Anal. Chem.* **2007**, *79*, 782−787.
(16) Minot, E. D.; Janssens, A. M.; Heller, I.; Heering, H. A.; Dekker, C.; Lemay, S. G. *Appl. Phys. Lett.* **2007**, *91*, 093507.
(17) Dekker, C. *Phys. Today* **1999**, *52*, 22−28.
(18) Chen, R. J.; Bangsaruntip, S.; Drouvalakis, K. A.; Kam, N. W. S.; Shim, M.; Li, Y.; Kim, W.; Utz, P. J.; Dai, H. *Proc. Nat. Acad. Sci. U.S.A.* **2003**, *100*, 4984−4989.
(19) Heller, I.; Kong, J.; Heering, H. A.; Williams, K. A.; Lemay, S. G.; Dekker, C. *Nano Lett.* **2005**, *5*, 137−142.
(20) Männik, J.; Goldsmith, B. R.; Kane, A.; Collins, P. G. *Phys. Rev. Lett.* **2006**, *97*, 016601.
(21) Allen, B. L.; Kichambare, P. D.; Star, A. *Adv. Mater.* **2007**, *19*, 1439−1451.
(22) Cui, Y.; Wei, Q.; Park, H.; Lieber, C. M. *Science* **2001**, *293*, 1289−1292.
(23) Patolsky, F.; Lieber, C. M. *Mater. Today* **2005**, *8*, 20−28.
(24) Curreli, M.; Li, C.; Sun, Y.; Lei, B.; Gundersen, M. A.; Thompson, M. E.; Zhou, C. *J. Am. Chem. Soc.* **2005**, *127*, 6922−6923.
(25) Bard, A. J.; Faulkner, L. R. *Electrochemical Methods, Fundamentals and Applications.*, 2nd ed.; John Wiley & Sons: New York, 2001.
(26) Heller, I.; Kong, J.; Williams, K. A.; Dekker, C.; Lemay, S. G. *J. Am. Chem. Soc.* **2006**, *128*, 7353−7359.
(27) Alberts, B.; et al. *Molecular Biology of The Cell*, 3rd ed.; Garland Publishing, Inc.: New York, 1994.
(28) Tans, S. J.; Verschueren, A. R. M.; Dekker, C. *Nature* **1998**, *393*, 49−52.
(29) Rosenblatt, S.; Yaish, Y.; Park, J.; Gore, J.; Sazonova, V.; McEuen, P. L. *Nano Lett.* **2002**, *2*, 869−872.
(30) Dürkop, T.; Getty, S. A.; Cobas, E.; Fuhrer, M. S. *Nano Lett.* **2004**, *4*, 35−39.
(31) Heinze, S.; Tersoff, J.; Martel, R.; Derycke, V.; Appenzeller, J.; Avouris, P. *Phys. Rev. Lett.* **2002**, *89*, *106801*.
(32) Chen, Z.; Appenzeller, J.; Knoch, J.; Lin, Y.; Avouris, P. *Nano Lett.* **2005**, *5*, 1497−1502.

NL072996I